

## POSS/PDMS MMMs with reversal trade-off effect: characterization and enhanced permeation flux

Xia Zhan<sup>a,c,\*</sup>, Teng Gao<sup>a</sup>, Juan Lu<sup>b,\*</sup>, Jihui Liu<sup>a</sup>, Mengyan Wang<sup>a</sup>, Jiding Li<sup>c</sup>

<sup>a</sup>Key Laboratory of Cleaner Production and Integrated Resource Utilization of China National Light Industry, Beijing Technology and Business University, Beijing 100048, China, emails: zhanxia@th.btbu.edu.cn (X. Zhan)

<sup>b</sup>The Institute of Medicinal Plant Development, the Chinese Academy of Medical Sciences (CAMS) and Peking Union Medical College (PUMC), Beijing 100193, China, email: jlu@implad.ac.cn (J. Lu)

<sup>c</sup>The State Key Laboratory of Chemical Engineering, Department of Chemical Engineering, Tsinghua University, Beijing 100084, China, email: lijiding@mail.tsinghua.edu.cn (J. Li)

Received 7 August 2019; Accepted 4 January 2020

### ABSTRACT

In designing mixed-matrix membranes (MMMs) to overcome the trade-off effect of pervaporation performance, compatibility between filler and polymer, filler particle size and porous structure, and homogeneous filler distribution are important factors. In this contribution, nano-scale otca vinyl-polyhedral oligomeric silsesquioxanes (OV-POSS) was incorporated into polydimethylsiloxane (PDMS) to prepare OV-POSS/PDMS MMMs for pervaporation separation of ethanol/water mixtures. The morphology and physicochemical properties of the POSS/PDMS MMMs were characterized by scanning electron microscope, Fourier transform infrared spectroscopy, X-ray diffraction, Differential Scanning Calorimetry, Thermal gravimetric analysis, vapor adsorption, and swelling degree measurements. It was found that POSS dispersed homogeneously in the PDMS matrix and maintained good integration with PDMS with POSS loading below 10 wt.% due to the soluble properties of POSS in solvent and similar Si–O–Si structure in POSS and PDMS molecules. Compared with pure PDMS membrane, POSS/PDMS MMMs broke through trade-off effect and exhibited both higher permeation flux and separation factor, contributed by the porous OV-POSS and loose packing of PDMS chains with enhanced sorption and diffusion selectivity. The MMMs with only 1.59 wt.% POSS loading showed the best performance with the optimal flux of 2200 g/m<sup>2</sup>h (243% higher than that of pure PDMS) and corresponding separation factor of 9.3 (31% higher than that of pure PDMS) at 60°C. The effect of operating temperature and ethanol concentration on membrane intrinsic microstructure and driving force, as well as pervaporation performance, was investigated. It was found that POSS/PDMS MMMs exhibited superior permeation flux with considerable separation factor to most other PDMS-based membranes, and might, therefore, shed valuable insights to the development of high-performance POSS-based MMMs for ethanol recovery.

**Keywords:** Otca vinyl-polyhedral oligomeric silsesquioxanes; Polydimethylsiloxane; Reversal trade-off effect; Pervaporation; Permeation flux

### 1. Introduction

Ethanol biofuel has been caught widespread concentration around the world due to its renewable and clean

properties for bolstering energy security and sustainability. However, the main challenge was the ethanol prohibited effect in the biological fermentation process [1–3]. As ethanol concentration reached 8–10 wt.%, the fermentation process was inhibited by ethanol, and the continuous ethanol

\* Corresponding authors.

production was hindered. And so the ethanol product with low concentration should be recovered from the fermentation broth. Nowadays, distillation has been usually used for ethanol recovery with high energy consumption and production cost. The separation and purification steps accounted for 60%–80% of the total production cost of most mature chemical processes [3]. Compared with distillation, pervaporation was an important alternative method due to low energy consumption and easiness to be coupled with fermentation broths, which can significantly improve fermentation productivity and production rate by alleviating the product prohibited effect [4–7].

Polydimethylsiloxane (PDMS) was considered to be the most prospective candidate for ethanol recovery from aqueous solution as it was cheap, easily accessible, and with large free volume [5–10]. However, pure PDMS membranes have encountered enormous challenges with respect to break through the trade-off effect between permeation flux and separation factor. Mixed matrix membranes (MMMs) have evolved as an excellent candidate to dissolve this problem [11–29]. Typical MMMs consist of a dispersed phase (e.g., silicalite-1 [12–18], zeolite socony mobil (ZSM-5) zeolite [19–20], metal organic framework (MOFs) [21–27], and organophilic nano-silica (ONS) [28,29], etc.) and a continuous polymeric phase (e.g., PDMS, poly(ether-block-amide) (Pebax) and polyvinylidene fluoride (PVDF), etc.). To fully play the role of molecular molecule-selective properties of inorganic fillers, much efforts have been devoted to increasing the loading amount of fillers to further improve the membrane performance.

Jia et al. [14] prepared Silicalite-1/PDMS MMMs, which showed an optimal separation factor of 59 with 77 wt.% zeolite loading and the corresponding permeation flux was only 89 g/m<sup>2</sup>h. Zhuang et al. [16] prepared silicalite-1/PDMS MMMs and obtained the highest separation factor of 34.3 with 67 wt.% silicalite-1 loading. Vane et al. [19] fabricated zeolite filled PDMS MMMs and reported an increase in ethanol/water selectivity of 400% with 65 wt.% ZSM-5 loading. Li et al. [26] prepared zeolitic imidazolate frameworks (ZIF-71)/PDMS MMMs for recovery of ethanol via pervaporation and MMMs with 20 wt.% ZIF-71 loading presented optimum pervaporation performance with a separation factor of 9.5 and permeation flux of 900 g/m<sup>2</sup>h. Xu et al. [23] fabricated hydrophobically modified ZIF-90/PDMS MMMs which exhibited enhanced morphology homogeneity and separation performance. The MMMs with 2.5 wt.% ZIF-90 loading showed the best performance with the optimal flux of 99.5 g/m<sup>2</sup>h and corresponding separation factor of 15.1 at 60°C. Mao et al. [24] reported in situ fabrication of ZIF-8 nanoparticles in PDMS membrane via interfacial synthesis and the resultant membrane exhibited a superior pervaporation performance with relatively high permeation flux (1,778 g/m<sup>2</sup>h) and comparable separation factor (12.1) with ZIF-8 loading in the range of 12.2–20.4 wt.%.

It was proved that MMMs with high filler loading could provide enhanced pervaporation performance as reported in literatures [15–24]. However, at high loadings, it was rather difficult for MMMs to maintain the processability for a thin and defect-free active layer with high selectivity. The incompatibility of inorganic and polymeric phase and aggregation of the fillers often resulted in non-selective interfacial voids

and limited the true exploitation of MMMs [22]. Under these cases, molecular diffusion tended to circumvent the fillers and instead passed through non-selective interfacial voids, consequently sacrificing the membrane selectivity. And so in designing MMMs to overcome the trade-off effect of pervaporation performance, compatibility between filler and polymer, filler particle size, and porous structure, as well as homogeneous filler distribution were critical factors to achieve ideal pervaporation performance. Besides, it may be an alternative choice to find an effective filler with low filler loading to improve membrane performance, which can easily avoid the issues caused by high filler loading.

In recent years, polyhedral oligomeric silsesquioxane (POSS) has been caught great attention due to its nano-scale cage-like organic/inorganic hybrid structure [30]. The organic groups bonded to the inorganic –Si–O– framework made it possible to composite with polymer at the molecular level [30–32]. Moreover, unlike other inorganic particles, such as silica and zeolite, POSS was soluble in common solvents, such as Tetrahydrofuran (THF) and acetone, which were also good solvents for PDMS. It also provided the possibility for good compatibility between POSS and PDMS. POSS nanostructure and its outstanding unique advantages also made POSS a promising candidate in membrane application [33–43], including gas separation, pervaporation, and forward osmosis. Le et al. [33] prepared POSS/Pebax MMMs for ethanol recovery and found that the incorporation of POSS could break through the trade-off effect with low POSS loading (2 wt.%). However, the maximum permeation flux and separation factor of MMMs was still at a low level (183.5 g/m<sup>2</sup>h and 4.6, respectively). And so it might be very necessary to choose proper polymer and POSS filler with good compatibility to achieve higher pervaporation performance. Liu et al. [34] found that methyl-POSS could finely control the conformation and topology of PDMS polymer chains with molecular-interaction-driven tunable free volumes. As applied to the bio-butanol recovery from aqueous solutions, the prepared POSS/PDMS MMMs exhibited a simultaneous increase in permeability and selectivity. Zhang et al. [35] also prepared methyl-POSS/PDMS MMMs and applied for desulfurization. It was found that the MMMs had an excellent promising application in pervaporation separation of thiophene from n-heptane, which agreed with the solubility and diffusion behavior obtained by inverse gas chromatography study. Our group [43] proposed octa[(trimethoxysilyl)ethyl]-polyhedral oligomeric silsesquioxane (OPS) cross-linked PDMS MMMs to enhance pervaporation separation performance of ethanol/water mixtures. The separation factor of OPS/PDMS MMMs reached the maximum value of 16.4, while the permeation flux was still at a low level of 253 g/m<sup>2</sup>h. In addition, the investigation of finely tuning PDMS membrane properties by POSS with different functional groups is still limited, and the enhancement on membrane separation performance has not been fully exploited.

In this study, octa vinyl-polyhedral oligomeric silsesquioxanes (OV-POSS) as shown in Fig. 1, was incorporated into hydrophobic PDMS to prepare POSS/PDMS MMMs. OV-POSS and PDMS maintained similar hydrophobic properties and Si–O–Si structures. It was expected that the incorporation of POSS into PDMS could overcome the

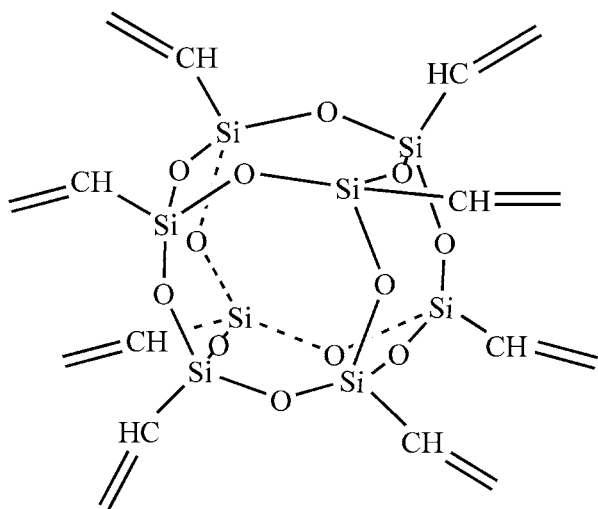


Fig. 1. Molecular structure of OV-POSS.

shortcomings of common inorganic/organic MMMs in dispersion and compatibility aspects and make full use of fast transport pathways induced by porous POSS particles to obtain higher permeation flux. The morphology, chemical and crystalline structures, thermal properties vapor adsorption properties, and swelling properties of POSS/PDMS MMMs were characterized. The effect of POSS loading, operation temperature, and ethanol feed concentration on pervaporation performance were also investigated in detail. This work may provide a useful database and roadmap for the fabrication of POSS-containing MMMs in the application of biofuel recovery via pervaporation.

## 2. Experimental

### 2.1. Materials

OV-POSS was purchased from Liaoning Am Union Composite Materials Co., Ltd (Shenyang of Liaoning Province, China). PDMS (107, 20,000 mPa s) was provided by Beijing Chemical Reagents Corporation. THE, di-n-butyltindilaurate (DBTL), pentane, Tetraethoxysilane (TEOS), and ethanol were obtained from Beijing Jingyi Chemical Reagents Corporation and were used as received. The PVDF porous membrane was prepared by our laboratory and the preparation process was described in detail elsewhere [8].

### 2.2. Preparation of POSS/PDMS membranes

Appropriate amount of PDMS was added in THF and agitated for 30 min to obtain homogeneous PDMS solution (A solution). And then appropriate amount of OV-POSS was added in THF solvent, with magnetic stirring for 1 h and ultrasonic agitation for another 30 min to form another solution (B solution). A and B solution mixed together with magnetic stirring for another 1 h. The cross-linking reagent TEOS and catalyst DBTL was added into the solution to initiate pre-polymerization, with continuous magnetic stirring to obtain a homogeneous and viscous solution. The solution was cast on PVDF porous support to obtain POSS/PDMS-PVDF composite membranes and cast on PTFE plate to

obtain POSS/PDMS homogeneous membranes. The primary membranes were laid in an oven at 80°C for 5 h to achieve complete cross-linking. The weight ratio of PDMS: THF: TEOS: DBTL was 30:70:3:1.2. To make a comparison, the pure PDMS membrane was also prepared according to the above weight ratio. The weight ratio of POSS:(PDMS+POSS) was 1.59, 5.00, 10.00, 15.00, and 18.41 wt.%, respectively, which was defined as POSS loading.

### 2.3. Characterization

Infrared spectra of the OV-POSS particles and membrane samples were measured with a Nicolet IR560 infrared analyzer. Morphological studies were performed on a scanning electron microscope (SEM, JEOL JSM-7401F) at a voltage of 3.0 kV. The crystallization of OV-POSS particles and membrane samples were characterized with X-ray diffractometer (Rigaku D/max-2550) with mono-chromatized Cu K $\alpha$  radiation. Thermal gravimetric analysis (TGA) was carried out on a Thermal gravimetric analysis Instruments (STA409 C/3/F). The pure ethanol, water vapor adsorption properties into OV-POSS/PDMS MMMs were measured with ASAP2020 volumetric gas adsorption apparatus equipped with a vapor generation accessory at 20°C.

Swelling degree (SD) was measured by calculating the equilibrium liquid uptake of homogeneous membranes in 10 wt.% ethanol/water mixtures at 20°C. The SD was calculated according to the following equation,  $SD = (m_1 - m_0)/m_0$ , where  $m_0$  and  $m_1$  referred to the mass of the dry membrane and the swollen membrane at equilibrium, respectively. Gel content was generally used to measure the mass ratio of cross-linked parts to the whole membrane. A certain amount of dry POSS/PDMS MMMs were weighed ( $m_2$ ) and immersed in toluene for 48 h at 20°C, and then was heated in an oven for 12 h at 100°C to a constant weight ( $m_3$ ). The ratio of  $m_2$  and  $m_3$  was defined as gel content.

### 2.4. Pervaporation performance measurement

The pervaporation performance was measured with a pervaporation apparatus built by our own laboratory as shown in Fig. 2. The ethanol concentration in the feed and permeate was measured by gas chromatography (GC-14C, Shimadzu). The ethanol feed concentration varied from 5 to 25 wt.%, and the operation temperature varied from 40°C to 80°C. In this study, permeation flux ( $J$ ), separation factor ( $\alpha$ ), permeability ( $P$ ), and membrane selectivity ( $\beta$ ) were used to evaluate the pervaporation performance of POSS/PDMS MMMs. The four parameters were defined as follows [19,33].

$$J = \frac{Q}{A \times t} \times \frac{l}{10} \quad (1)$$

The ethanol, water ( $J$ , g/m<sup>2</sup>h), and total fluxes ( $J$ , g/m<sup>2</sup>h) were normalized to a membrane thickness of 10  $\mu$ m unless otherwise specified, assuming an inverse proportionality between the total flux and the membrane thickness. Where  $Q$  (g) was the total mass of permeate collected in  $t$  hours, and  $A$  (m<sup>2</sup>) denoted the effective area of the membrane, and  $l$  was the membrane thickness of the selective layer.

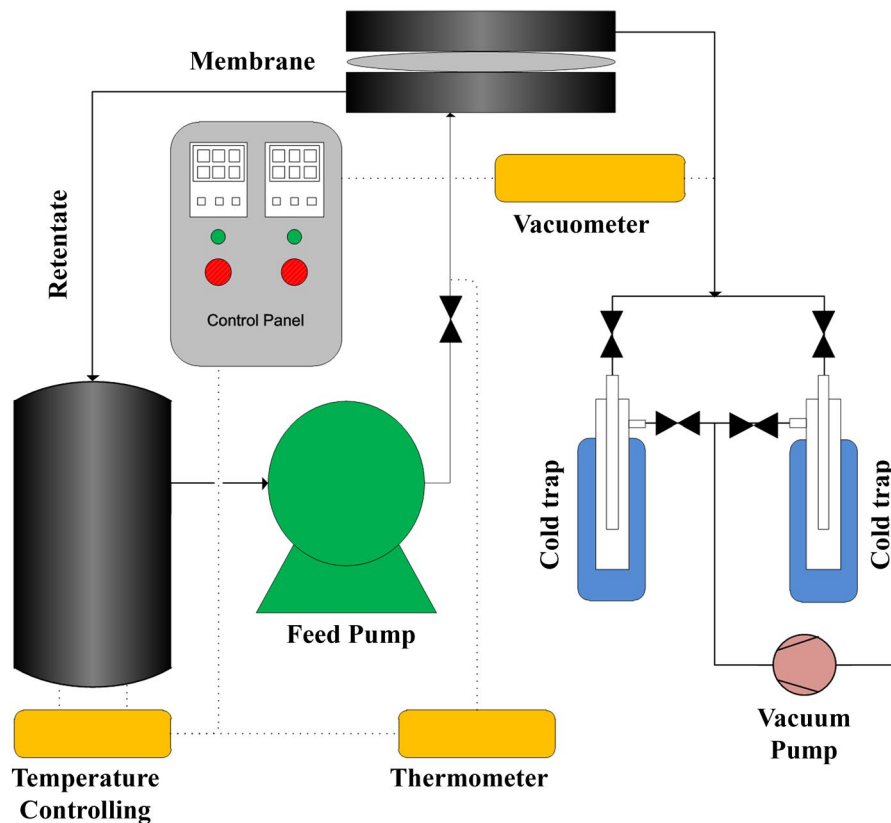


Fig. 2. Schematic diagram of the pervaporation apparatus.

$$\alpha = \frac{y_A \times x_B}{y_B \times x_A} \quad (2)$$

where  $x_A$  and  $x_B$  represented the ethanol and water concentrations (wt.%) in the feed solution respectively, and  $y_A$  and  $y_B$  represented the ethanol and water concentrations (wt.%) in the permeate.

Permeability ( $P_i$ ) and membrane selectivity ( $\beta$ ) were also calculated, which decoupled the effect of operation parameters and concentrated on the influence of the intrinsic membrane properties on pervaporation performance.

$$P_i = J_i \frac{10}{x_{n,i} \gamma_i P_i^{\text{sat}} - y_{n,i} P^p} \quad (3)$$

$$\beta = \frac{P_i}{P_j} \quad (4)$$

$$\alpha = \beta \times \frac{M_i}{M_j} \times \frac{P_j^{\text{sat}}}{P_i^{\text{sat}}} \times \frac{\gamma_i}{\gamma_j} \quad (5)$$

where  $J_i$  was the component  $i$  flux,  $x_{n,i}$  and  $y_{n,i}$  were the mole fractions of component  $i$  in the feed and in the permeate, respectively.  $\gamma_i$  was the activity coefficient,  $P_i^{\text{sat}}$  was the saturated vapor pressure, and  $P^p$  was the permeate pressure.

The driving force of component  $i$  to transport across the membrane could be described as Eq. (6). As the permeate pressure was controlled below 200 Pa, the  $y_{n,i} P^p$  in the driving force could be ignored. The driving force could be expressed as fugacity ( $f_i$ ) which was the partial vapor pressure of component  $i$  at the feed side.

$$\text{driving force} = x_{n,i} \gamma_i P_i^{\text{sat}} - y_{n,i} P^p \quad (6)$$

### 3. Results and discussion

#### 3.1. FT-IR spectra of POSS/PDMS MMMs

As shown in Fig. 3, the infrared spectra of OV-POSS powder, PDMS, and POSS/PDMS MMMs were recorded by transmission and attenuated total reflection (ATR) technique, respectively. The characteristic bands of OV-POSS at 3,069 and 3,024  $\text{cm}^{-1}$  were assigned to the stretching vibrations of C=C–H [31]. The characteristic bands of OV-POSS at 1,605  $\text{cm}^{-1}$ , which was assigned to the stretching vibrations of C=C structure [31,43], didn't appear in the spectra of POSS/PDMS MMMs even with POSS loading as high as 18.41 wt.%. And there was no new characteristic absorption peak that appeared compared with the spectrum of pure PDMS [10,31]. This might be ascribed to that PDMS molecules covered almost the entire surface of hybrid membranes because PDMS' low surface free energy drove the PDMS segment to segregate to the free surface. The characteristic absorption

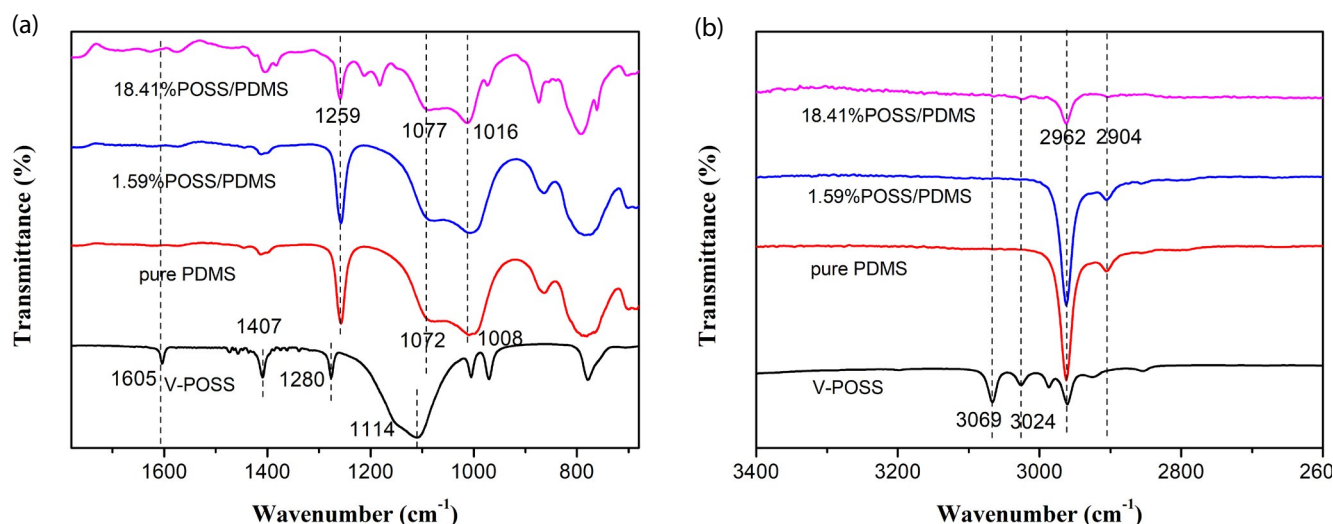


Fig. 3. (a and b) FT-IR spectra of OV-POSS, pure PDMS, and OV-POSS/PDMS MMMs.

peaks of OV-POSS particles covered with PDMS molecules might not be detected on account of the ATR detecting depth of several micrometers [44,45]. The characteristic absorption peaks of asymmetric Si–O–Si stretching vibration in OV-POSS was around  $1,114\text{ cm}^{-1}$ . The band around  $1,072\text{ cm}^{-1}$  in PDMS membrane was assigned to the asymmetric Si–O–Si stretching vibration, and the band at  $1,008\text{ cm}^{-1}$  was generally considered to be resulted from the random structure of the asymmetric Si–O–Si stretching vibration [31,46]. It can be seen that the asymmetric Si–O–Si stretching vibration band around  $1,072$  and  $1,008\text{ cm}^{-1}$  in pure PDMS shifted to higher frequencies ( $1,077$  and  $1,016\text{ cm}^{-1}$ , respectively) in MMMs with 18.41 wt.% POSS loading. The blue shift might be attributed to the combined effect of the characteristic peaks of PDMS and OV-POSS, and the presence of molecular interactions between POSS and PDMS due to similar Si–O–Si structure [31,33,34].

### 3.2. Morphology of POSS/PDMS MMMs

Figs. 4–6 showed the morphologies of OV-POSS particles, pure PDMS, and POSS/PDMS MMMs. As shown in Fig. 4, although OV-POSS was a kind of nano-sized particles, a large number of POSS particles always assembled and formed much larger POSS aggregates without any treatment.

Larger POSS aggregates maintained lower surface energy and higher stability but might bring difficulties to achieve homogeneous dispersion of OV-POSS into PDMS matrix. And so, OV-POSS was added in THF solvent separately in the preparation process of hybrid membranes, with magnetic stirring for 1 h and ultrasonic agitation for another 30 min to achieve changes from POSS aggregates to individual particles and dissolution of POSS particles. As shown in Figs. 5 and 6, there was no large POSS aggregates on the surface or in the cross-section of OV-POSS/PDMS MMMs, which illustrated that magnetic stirring and ultrasonic agitation could effectively transfer POSS aggregates into POSS particles in THF solvent.

It was found that the surface and cross-section of the POSS/PDMS selective layer were dense and without pinholes. As POSS loading was below 10 wt.%, POSS particles dispersed homogeneously in the PDMS matrix and integrated with PDMS tightly (as shown in Figs. 5 and 6). This may be attributed to two factors. First, OV-POSS was soluble in THF solvent. Second, the similar Si–O–Si structure may create interaction between POSS and PDMS [33,34]. As POSS loading increased furthermore, small POSS aggregates became obvious on the surface, but POSS and PDMS still maintained good integration. This revealed the POSS/PDMS MMMs with appropriate POSS loading could overcome the

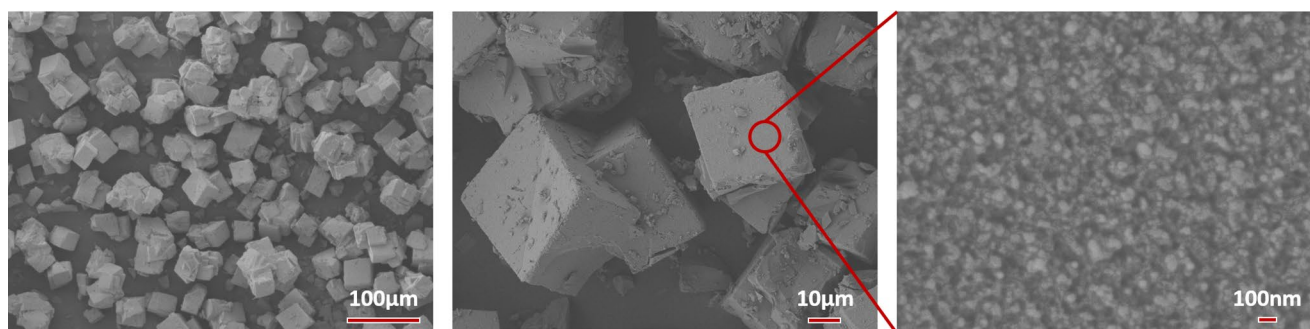


Fig. 4. SEM images of OV-POSS particles with different magnification.

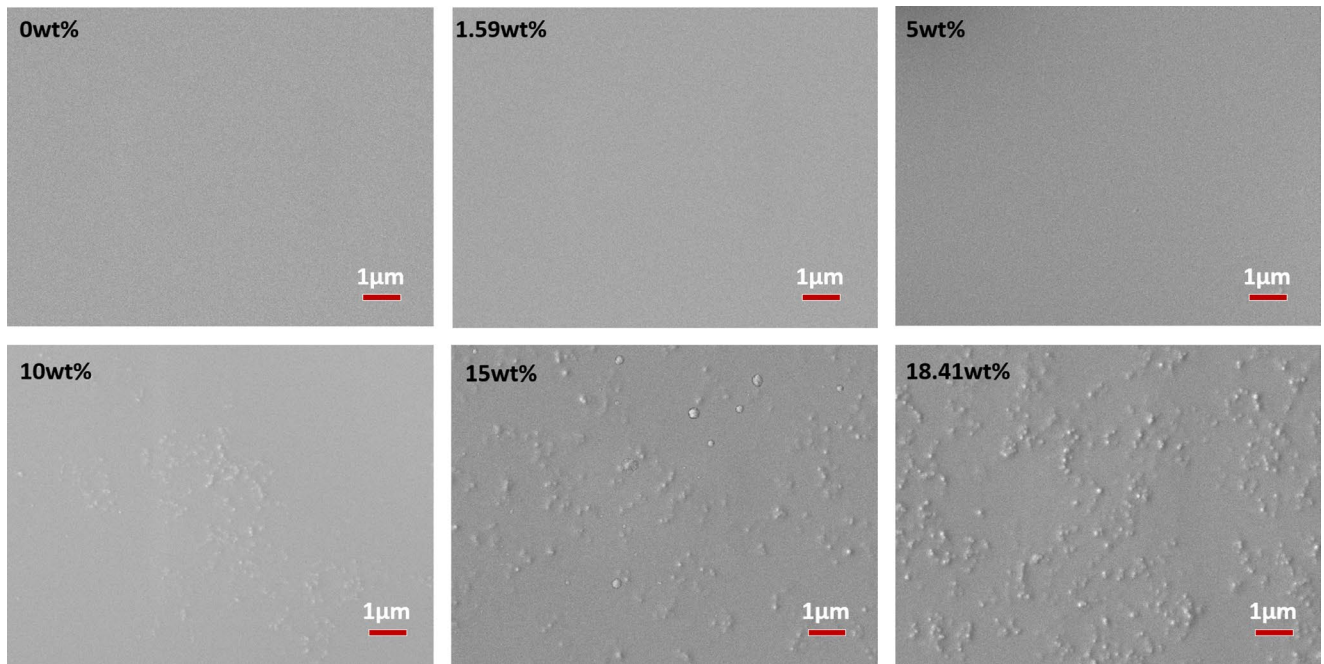


Fig. 5. SEM images of surface of OV-POSS/PDMS MMMs with different POSS loading.

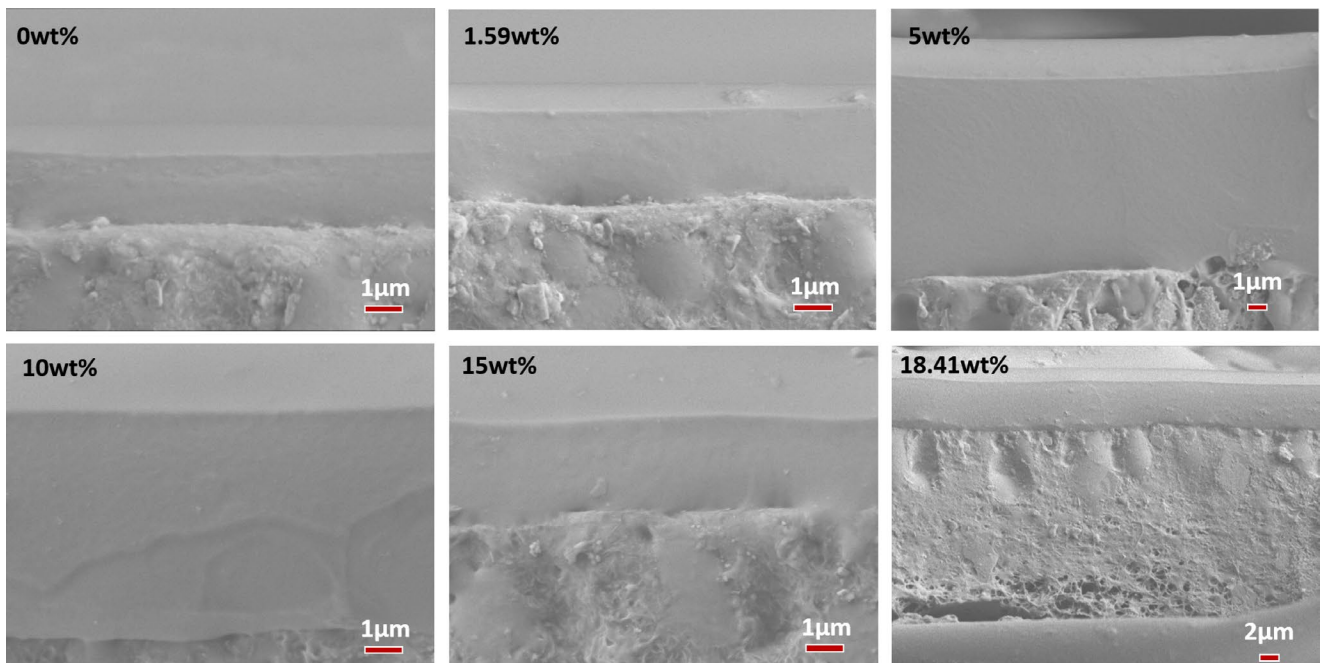


Fig. 6. SEM images of cross-section of OV-POSS/PDMS MMMs with different POSS loading.

shortcomings of common inorganic/organic hybrid membranes in dispersion and integration aspects.

### 3.3. X-ray diffraction spectra analysis of POSS/PDMS MMMs

Fig. 7 shows the X-ray diffraction (XRD) spectra of OV-POSS, PDMS, and POSS/PDMS MMMs. The diffused diffraction peak between  $10^\circ$  and  $15^\circ$  revealed that pure

PDMS had a typical amorphous structure with partial crystalline domains, which was similar to those reported in literature [31,43,47]. The sharp diffraction peaks at  $9.9^\circ$ ,  $13.2^\circ$ ,  $19.7^\circ$ ,  $21.1^\circ$ ,  $22.9^\circ$ , and  $23.8^\circ$  was attributed to the characteristic crystallization peaks of OV-POSS [31]. In the XRD spectra of POSS/PDMS MMMs, both kinds of characteristic diffraction peaks appeared. And as the POSS loading increased, the intensity and number of sharp

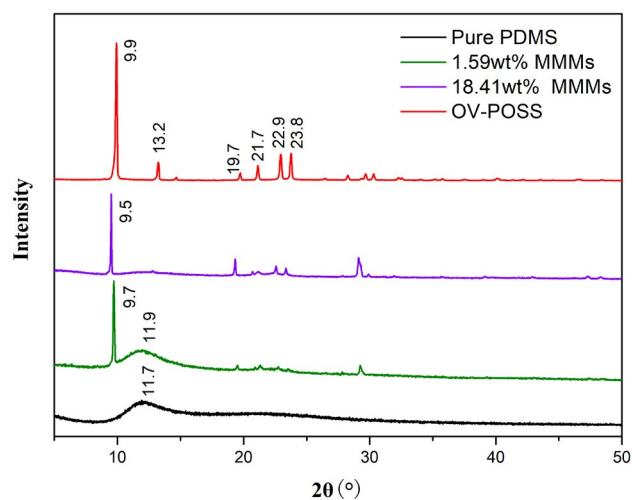


Fig. 7. XRD spectra of OV-POSS, pure PDMS and OV-POSS/PDMS MMMs.

diffraction peaks increased, while the intensity of the diffused diffraction peak decreased. As POSS loading reached 18.41 wt.%, the diffused diffraction peak of PDMS almost disappeared, which illustrated more POSS particles disrupted partial orderly arrangement of PDMS chains and resulted in much lower crystalline degree of PDMS chains. More amorphous region was formed by the loose packing structure of PDMS chains. The diffused diffraction peak of PDMS shifted slightly to 11.9° (in 1.59 wt.% POSS/PDMS MMM) from 11.7° (in pure PDMS membrane). According to Bragg Equation, this revealed that the incorporation of POSS decreased the inter-planar spacing of PDMS chains. This might be ascribed to the reduced chain mobility and denser chain packing of PDMS chains in the vicinity of dispersed POSS nanoparticles, which was proposed as a chain rigidification effect [34,47,48]. The sharp intense peak at 2-theta of 9.8 in OV-POSS particles shifted slightly to a lower degree in hybrid membranes (9.7° and 9.5°), which might indicate that PDMS molecular chains strongly interact with POSS particles and enlarge the inter-planar spacing of POSS slightly. Liu et al. [34] also found that the crystalline POSS was slightly affected by the PDMS matrix, resulting in a 0.1°–0.2° shifting of the characteristic peaks in XRD.

### 3.4. Thermal properties of POSS/PDMS MMMs

To investigate the effect of POSS on the thermal degradation properties of PDMS membranes, TGA, and Differential Scanning Calorimetry measurements for various samples were conducted as shown in Figs. 8 and 9. It was found that the degradation step among 200°C–300°C was observed for OV-POSS, which was resulted from the degradation of vinyl groups and Si–O framework. The final weight loss of OV-POSS was about 88 wt.%. The degradation of pure PDMS membrane began from 300°C, and the final weight loss was almost 100 wt.% as the temperature reached 780°C. As the POSS loading increased, the initial degradation temperature of MMMs decreased from 300°C to 200°C, which was ascribed to the degradation of OV-POSS at 200°C. The

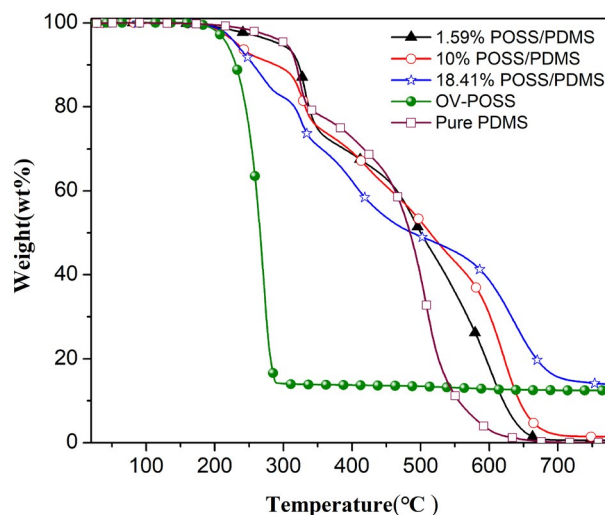


Fig. 8. The TG curves for OV-POSS and OV-POSS/PDMS MMMs with different POSS loading.

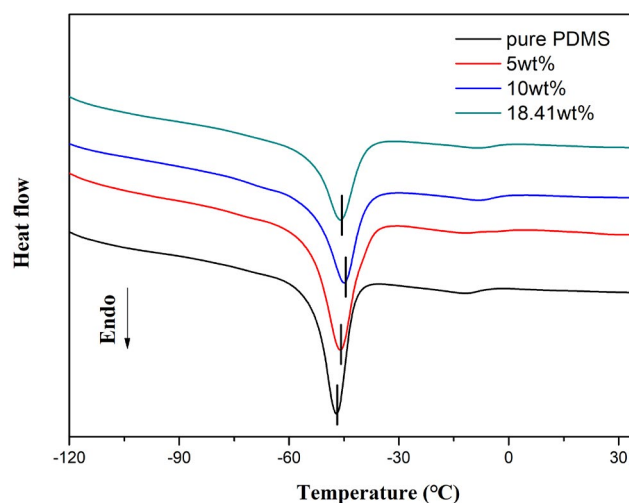


Fig. 9. Differential Scanning Calorimetry heating thermograms for pure PDMS membranes and OV-POSS/PDMS MMMs.

increased OV-POSS loading led to the lower initial degradation temperature of POSS/PDMS MMMs. However, the final weight loss decreased gradually with increasing POSS loading. Moreover, the degradation velocity of hybrid membranes slowed down obviously with increasing POSS loading as the temperature was above 500°C, which illustrated that the incorporation of POSS into PDMS could improve the thermal stability at high temperatures.

Melting temperature ( $T_m$ ) of PDMS crystallization provided an estimation of the flexibility of polymer chains [47,48]. The  $T_m$  of OV-POSS/PDMS MMMs was higher than that of pure PDMS as shown in Fig. 9. Similar results have been found in PDMS MMMs [47,48]. It was considered that the strong interaction between OV-POSS and PDMS chains and chain rigidification effect of PDMS chains in the vicinity of dispersed POSS nanoparticles contributed to the increase of  $T_m$ , which was consistent with the decreased inter-planar

spacing of PDMS chains in hybrid membranes as revealed by XRD.

### 3.5. Ethanol and water vapor adsorption

To investigate the sorption properties of pure ethanol/water in membranes, ethanol and water vapor adsorption properties of three homogeneous membranes were measured, including pure PDMS and OV-POSS/PDMS MMMs with POSS loading of 1.59 and 5 wt.%. As shown in Figs. 10a and b, OV-POSS/PDMS MMMs showed both higher ethanol vapor adsorption quantity and lower water vapor adsorption quantity than those of pure PDMS membrane. It was very interesting that the incorporation of OV-POSS into PDMS not only improved ethanol vapor adsorption, but also depressed water vapor adsorption of PDMS membranes. This suggested that OV-POSS was an effective filler to improve membrane sorption selectivity to ethanol. All membranes presented higher ethanol vapor adsorption quantity than water vapor adsorption quantity, which indicated that ethanol adsorption was before water adsorption on/in all the membranes.

### 3.6. Swelling properties

The SD and gel content of OV-POSS/PDMS MMMs was listed in Table 1. As POSS loading increased, the SD increased as well, while the gel content decreased. The decreased gel content might be ascribed to the migration of partial OV-POSS particles out of membranes in the swelling process. The SD of membranes was enhanced by the incorporation of OV-POSS into PDMS but was still below 5%, which met the requirements of swelling resistance in industrial applications. There were several factors affecting the SD: (1) porous OV-POSS particles and aggregates can hold a certain amount of feed solution; (2) the loose packing and decreased crystalline degree of PDMS chains resulted from lower inter-molecular interaction was beneficial to adsorption of small molecules; (3) the chain rigidification effect and

strong interaction between OV-POSS and PDMS chains can substantially restrain the stretching of the PDMS polymer chains, which partially offset the increase of SD. The former two factors played a dominant role in SD and resulted in the simultaneous growth with increasing POSS loading.

### 3.7. Pervaporation performance

#### 3.7.1. Effect of POSS loading on pervaporation performance

Fig. 11 shows the effect of POSS loading on pervaporation performance (60°C, [EtOH] = 10 wt.%, 10 μm). As shown in Fig. 11, the incorporation of POSS into PDMS could improve separation factor and permeation flux simultaneously, which exhibited a reversal trade-off effect. The permeation flux was significantly increased from 641 to 2200 g/m<sup>2</sup>h by incorporating 1.59 wt.% OV-POSS into the PDMS matrix, with separation factor increasing slightly from 7.1 to 9.3. The reason was considered that porous OV-POSS and loose packing of PDMS chains contributed to much higher absorption uptakes and diffusion rate of small molecules. The porous POSS cages and loose packing of PDMS chains provided more and larger cavities which were beneficial to preferential absorption and diffusion of ethanol molecules, as the molecular size of ethanol (0.46 nm) was larger than that of water molecules (0.32 nm) [33].

However, as POSS loading increased furthermore, both the separation factor and permeation flux decreased.

Table 1  
Characterization of swelling properties of POSS/PDMS homogeneous membranes

Membranes	POSS loading (wt.%)					
	0	1.59	5	10	15	18.41
SD (%)	2.1	4.0	4.3	4.7	4.9	4.9
Gel content (%)	92.6	92.0	91.8	91.3	90.7	89.4

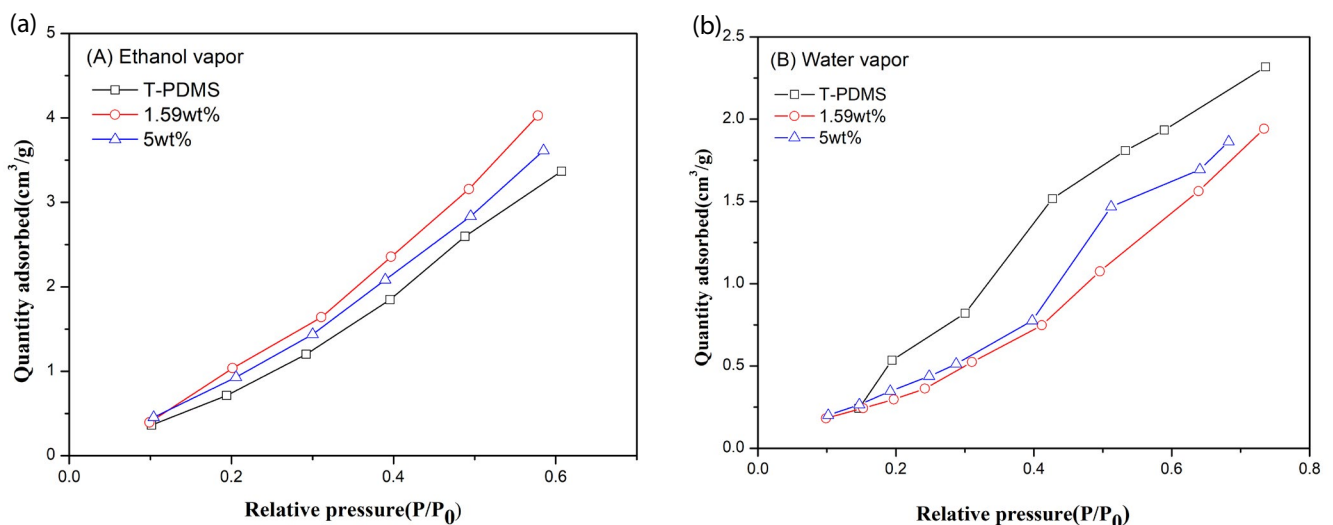


Fig. 10. (a) Ethanol and (b) water vapor adsorption isotherms of OV-POSS/PDMS MMMs with different POSS loading.

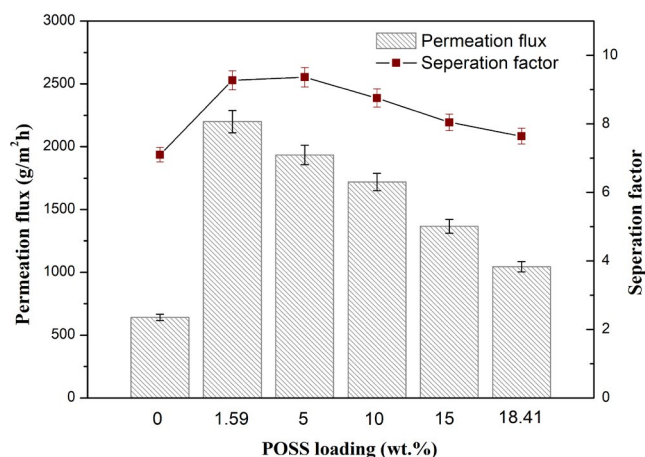


Fig. 11. Effect of POSS loading on pervaporation performance of hybrid membranes.

Since the variation tendency of permeation flux of hybrid membranes caused by increasing POSS loading was opposite of that of SD, it was presumed that the diffusion process rather than sorption process was the rate-determining step in pervaporation. The main control factor might be the long and tortuous diffusion path caused by the enhanced chain rigidification effect and intermolecular interactions between the matrix and the POSS nanoparticles that increased transport resistance. Fig. 12 proposes a schematic diagram of ethanol/water transport pathways across pure PDMS membranes and OV-POSS/PDMS MMMs with different POSS loading. The strong interaction between OV-POSS and PDMS chains made POSS particles/aggregates surrounded by rigid PDMS chains, which depressed the fast transport across the interface and porous POSS particles. More OV-POSS could be only served as saturated reservoirs and couldn't provide fast transport pathways for small molecules, which led to a decrease of permeation flux with increasing POSS loading. Le et al. [33] also found the maximum permeation flux of POSS/Pebax was achieved at 2 wt.% POSS loading and a higher amount of POSS particles didn't lead to a higher flux. This indicated that only a small amount of POSS loading was needed to obtain optimum separation

performance, which was convenient to achieve large-scale industrial production.

### 3.7.2. Effect of operation temperature on pervaporation performance

Figs. 13–15 show the effect of operating temperature on pervaporation performance of POSS/PDMS MMMs ([EtOH] = 10 wt.%, POSS loading of 5%). As operation temperature increased, both ethanol and water flux increased (as shown in Fig. 13). It was generally considered that the increase of permeation flux with a temperature rising was attributed to the increase of free volume and chain segment movement rate of PDMS [9–12,28]. It was considered that permeation flux was determined by both intrinsic membrane structure and driving force. And so permeability was more accurate to reflect the influence of intrinsic membrane properties on permeation flux. As shown in Fig. 14, both ethanol and water permeability decreased with increasing operation temperature from 40°C to 60°C and almost kept constant in the range of 60°C–80°C, which was just the opposite with the variation tendency of permeation flux. This interesting result indicated that the increase of permeation flux with increasing temperature was mainly attributed to the increased external driving force (saturated vapor pressure) rather than a variation of intrinsic membrane property. Table 2 gives the effect of operating temperature on activity coefficient, saturated vapor pressure, and feed fugacity of ethanol/water mixture. As operation temperature increased, the external driving force (saturated vapor pressure, feed fugacity) increased sharply, which played a dominant role over the intrinsic properties of hybrid membranes in permeation flux increasing.

As shown in Fig. 15, the membrane selectivity of POSS/PDMS MMMs was around 2 and showed ethanol perm-selectivity in the range of 40°C–80°C. The separation factor increased firstly and then decreased with increasing operating temperature. In the range of 40°C–80°C, the separation factor varied between 7.6 and 9.3. It was considered that operation temperature had a great influence on ethanol/water sorption and diffusion behaviors, which finally determined the variation tendency of separation factor. The swelling of membrane and mobility of PDMS chains would

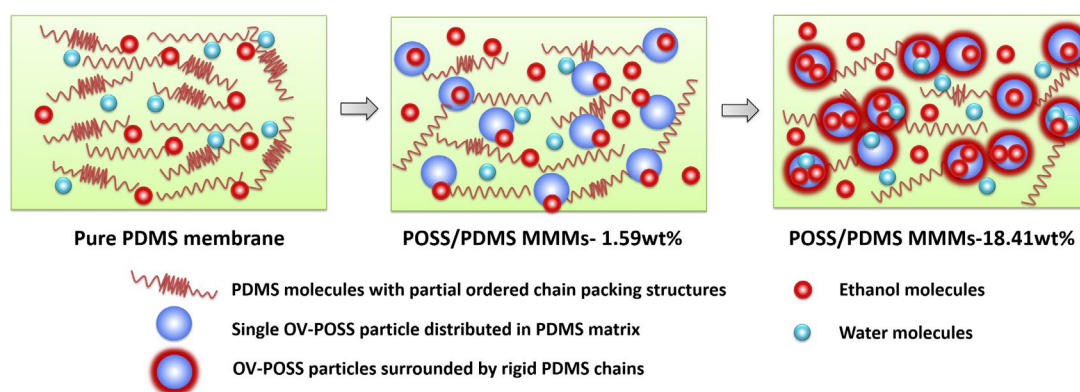


Fig. 12. Schematic diagram of ethanol/water transport pathways across pure PDMS membranes and OV-POSS/PDMS MMMs with different POSS loading.

be enhanced by increasing operation temperature, which might provide more and larger cavities for ethanol/water molecules. The enlarged cavities were beneficial to ethanol diffusion rather than water diffusion since the molecular size of ethanol (0.46 nm) was larger than that of water molecules

(0.32 nm) [33]. In addition, both OV-POSS and PDMS used in this study were hydrophobic, in which enlarged cavities resulted in a steeper rise of the sorption selectivity towards ethanol than that toward the water. Consequently, both increased sorption and diffusion selectivity contributed to the increased separation factor in the range of 40°C–50°C. However, as operation temperature reached 60°C, the cavity size in the hybrid membrane might exceed a critical value [11,34], and increasing cavity size furthermore would lead to a higher water diffusion rate rather than ethanol diffusion rate. Sun et al. [28] also found a similar phenomenon in diffusion properties of ONS/PDMS hybrid membranes. They found that the ethanol diffusion coefficient increased at a higher rate than that of water when the temperature was below 60°C, but when the temperature was 70°C, the ethanol diffusion coefficient increased at a lower rate than that of water. And so the depressed diffusion selectivity in the range of 60°C–80°C might play a dominant role over sorption selectivity improvement and consequently lead to the decline of separation factor.

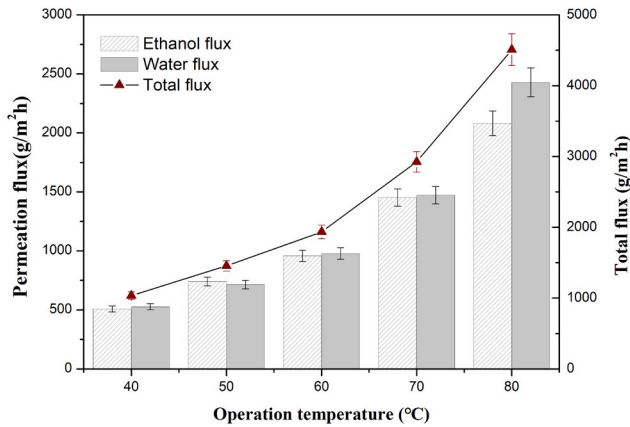


Fig. 13. Effect of operation temperature on permeation flux of OV-POSS/PDMS MMMs.

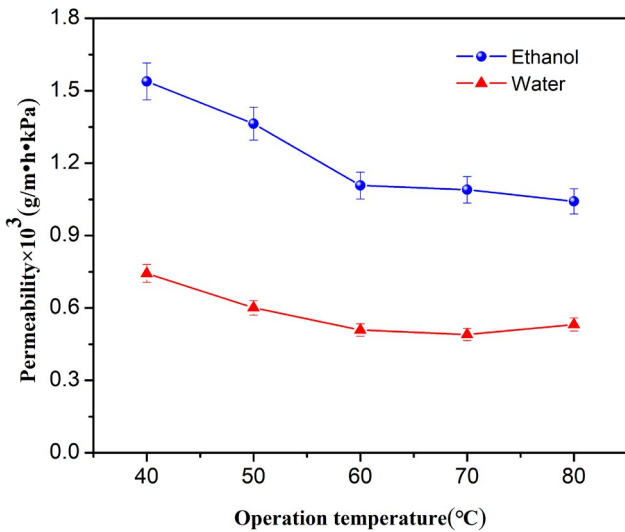


Fig. 14. Effect of operation temperature on permeability of OV-POSS/PDMS MMMs.

3.7.3. Effect of ethanol feed concentration on pervaporation performance

Figs. 16–18 show the effect of ethanol feed concentration on pervaporation performance of POSS/PDMS MMM (60°C,

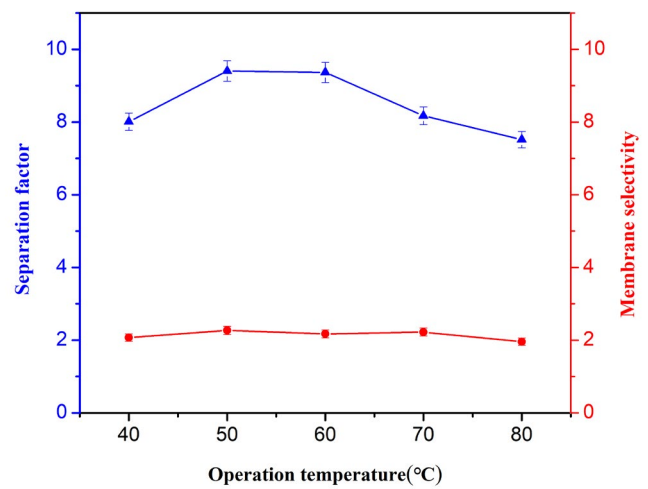


Fig. 15. Effect of operation temperature on separation factor and selectivity of OV-POSS/PDMS MMMs.

Table 2

Effect of feed temperature on activity coefficient, saturated vapor pressure and feed fugacity of ethanol/water (10 wt.%) mixture

Temperature (°C)	Activity coefficient		Saturated vapor pressure (kPa)		Feed fugacity (kPa)	
	Ethanol	Water	Ethanol	Water	Ethanol	Water
40			17.90	7.36	3.30	7.10
50			29.36	12.33	5.44	11.89
60	4.43	1.01	46.84	19.92	8.64	19.21
70			72.21	31.17	13.33	30.09
80			108.25	47.37	19.98	45.68

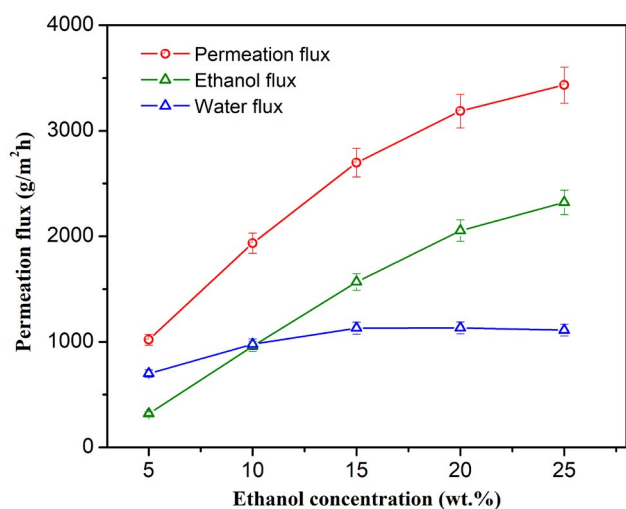


Fig. 16. Effect of ethanol feed concentration on permeation flux of OV-POSS/PDMS MMMs.

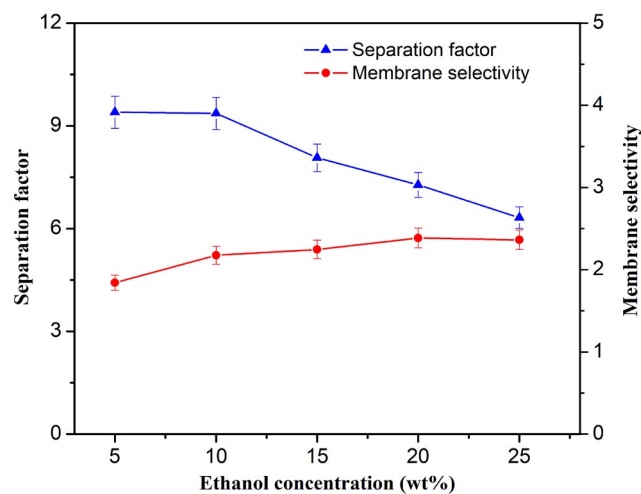


Fig. 18. Effect of ethanol feed concentration on separation factor and selectivity of OV-POSS/PDMS MMMs.

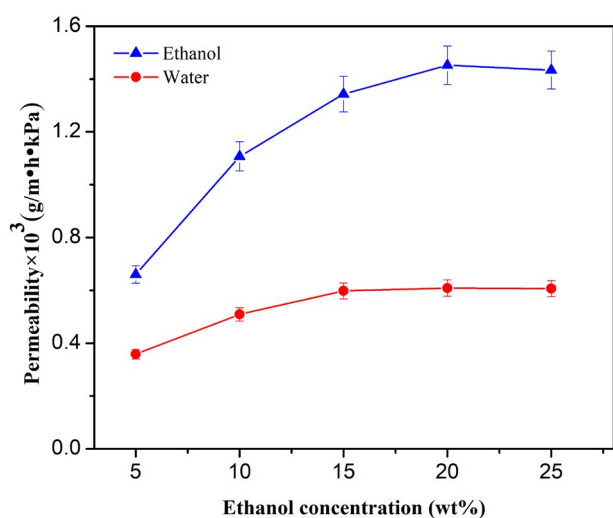


Fig. 17. Effect of ethanol feed concentration on permeability of OV-POSS/PDMS MMMs.

POSS loading of 5%). It was found that both ethanol and water flux increased with increasing ethanol concentration, and the ethanol flux increased more significantly than water flux. This was attributed to the increased driving force and free volume due to membrane swelling [43]. There were two aspects that influenced the water flux. The decrease of water molar ratio depressed the driving force of water transport, while the swelling of the membrane was beneficial to water absorption and diffusion. Two factors competed with each other and finally determined the inconspicuous rise of water flux.

As ethanol concentration increased, ethanol permeability increased more rapidly than water permeability, which resulted in the increase of membrane selectivity. It was probably contributed by the enhanced swelling of membranes which provided more and larger cavities beneficial

to preferential absorption and diffusion of ethanol molecules, as the molecular size of ethanol (0.46 nm) was larger than that of water molecules (0.32 nm). In the range of 5–25 wt.% ethanol concentration, the membrane selectivity was above 1, which indicated that POSS/PDMS MMM was ethanol perm-selective. As ethanol concentration increased, membrane selectivity increased, while the separation factor decreased. It was because the separation factor was not only influenced by membrane selectivity, but also by activity coefficient as shown in Eq. (5) [33]. As the ethanol concentration increased, the ethanol activity coefficient decreased significantly, and the water activity coefficient increased slightly (Table 3), which eventually led to the decrease of separation factor.

#### 3.7.4. Comparison of PV Performances of PDMS-Based Membranes

Table 4 summarized the PV performance of a number of typical PDMS based MMMs for ethanol recovery from aqueous solution. It can be seen that the permeation flux of most PDMS MMMs (except MOFs/PDMS MMMs) reported in literature was below 1,000 g/m<sup>2</sup>h. Silicalite-1 filled PDMS membranes showed the highest separation factor of 59 with permeation flux of only 89 g/m<sup>2</sup>h. Compared with pure PDMS and PDMS based MMMs, OV-POSS/PDMS MMMs with much lower POSS loading (1.59 wt.%) presented much higher permeation flux, which was beneficial to the large-scale production of PDMS based MMMs.

## 4. Conclusion

In summary, OV-POSS/PDMS MMMs were prepared and applied for ethanol recovery via pervaporation. It was found that POSS dispersed homogeneously with POSS loading below 10 wt.% and exhibited good compatibility with the PDMS matrix. As revealed by XRD and swelling measurement, it was found that the incorporation of OV-POSS into PDMS resulted in much looser PDMS chain packing

Table 3  
Effect of feed concentration on activity coefficient, saturated vapor pressure and feed fugacity at 60°C

Ethanol/water mixture (wt %)	Mole fraction (mol %)		Activity coefficient		Saturated vapor pressure (kPa)		Feed fugacity (kPa)	
	Ethanol	Water	Ethanol	Water	Ethanol	Water	Ethanol	Water
5/95	0.020	0.980	5.13	1.00			4.85	19.55
10/90	0.042	0.958	4.43	1.01			8.64	19.21
15/85	0.065	0.935	3.86	1.01	46.84	19.92	11.67	18.90
20/80	0.089	0.911	3.39	1.03			14.14	18.60
25/75	0.115	0.885	3.00	1.04			16.20	18.32

Table 4  
Comparison of PV performances of PDMS-based membranes

Hybrid membranes	Particle loading	Temperature (°C)	Separation factor	Permeation flux (g/m <sup>2</sup> h)	Refs.
ZSM-5/PDMS	65	50	43.1	40	[19]
Silicalite-1/PDMS	77	40	59	89	[14]
Silicalite-1/PDMS	60	22.5	16.5	51	[12]
Silicalite-1/PDMS	67	50	34.3	176	[16]
ONS/PDMS	5	60	30.1	114	[28]
ONS/PDMS	5	60	12.5	807	[29]
ZIF-8/PDMS	5	60	9.9	1229	[29]
ZIF-8/PDMS	–	40	12.1	1778	[24]
ZIF-90/PDMS	2.5	60	15.1	99	[23]
MCM-41@ZIF-8/PDMS	5	60	9.5	1846	[25]
ZIF-71/PDMS	20	50	9.5	900	[26]
OM-POSS/Pebax	2	25	4.6	184	[33]
OM-POSS/Pebax	2	25	4.1	126	[33]
OPS/PDMS	7.5	40	16.4	253	[43]
OV-POSS/PDMS	1.59	60	9.3	2200	This work
OV-POSS/PDMS	5	60	9.4	1935	This work
OV-POSS/PDMS	5	80	7.5	4509	This work

and enhanced SD. The vapor adsorption measurement suggested that the incorporation of OV-POSS into PDMS not only improved ethanol vapor adsorption, but also depressed water vapor adsorption of PDMS membranes, which might be beneficial to the selective sorption towards ethanol molecules.

OV-POSS/PDMS MMMs showed both higher permeation flux and separation factor than pure PDMS membrane, which presented the reversal trade-off effect. The MMMs with 1.59 wt.% POSS loading exhibited an optimal pervaporation performance with the permeation flux of 2200 g/m<sup>2</sup>h (243% higher than that of pure PDMS) and corresponding separation factor of 9.3 (31% higher than that of pure PDMS) at 60°C. The pronounced enhancement in separation performance could be attributed to the porous POSS cages and loose packing structure of PDMS chains, which might confer abundant entrances and construct rapid diffusion pathways for penetrant molecules. It was found that the increase of permeation flux with increasing temperature was mainly attributed to the increased external driving force (saturated

vapor pressure) rather than a variation of intrinsic membrane property. With increasing ethanol concentration, both ethanol/water permeation flux and permeability increased, and the ethanol permeability increased more rapidly than water permeability, which resulted in the increase of membrane selectivity. This study may serve as a novel approach to constructing rapid diffusion pathways in hybrid membranes by incorporating OV-POSS nanomaterials to surpass the trade-off effect between permeability and selectivity.

#### Acknowledgments

The authors greatly appreciate the financial support of Beijing Natural Science Foundation Commission-Beijing Municipal Education Commission joint Foundation (KZ201910011012), National Natural Science Foundation of China (21736001, 21776153, and 21206001), State Key Laboratory of Chemical Engineering, China (No. SKL-ChE-18A01), College Students Scientific Research and Undertaking Starting Action Project.

## References

- [1] C.H. Fu, D. Cai, S. Hu, Q. Miao, Y. Wang, P.Y. Qin, Z. Wang, T.W. Tan, Ethanol fermentation integrated with PDMS composite membrane: an effective process, *Bioresour. Technol.*, 200 (2016) 648–657.
- [2] S. Santoro, F. Galiano, J.C. Jansen, A. Figoli, Strategy for scale-up of SBS pervaporation membranes for ethanol recovery from diluted aqueous solutions, *Sep. Purif. Technol.*, 176 (2017) 252–261.
- [3] A.J. Ragauskas, C.K. Williams, B.H. Davison, G. Britovsek, J. Cairney, C.A. Eckert, W.J. Frederick Jr., J.P. Hallett, D.J. Leak, C.L. Liotta, J.R. Mielenz, R. Murphy, R. Templar, T. Tschaplinski, The path forward for biofuels and biomaterials, *Science*, 311 (2006) 484–489.
- [4] L.M. Vane, A review of pervaporation for product recovery from biomass fermentation processes, *J. Chem. Technol. Biotechnol.*, 80 (2005) 603–629.
- [5] P. Peng, B. Shi, Y. Lan, A review of membrane materials for ethanol recovery by pervaporation, *Sep. Sci. Technol.*, 46 (2010) 234–246.
- [6] L.M. Vane, Separation technologies for the recovery and dehydration of alcohols from fermentation broths, *Biofuels, Bioprod. Biorefin.*, 2 (2008) 553–588.
- [7] Y.K. Ong, G.M. Shi, N.L. Le, Y.P. Tang, J. Zuo, S.P. Nunes, T.S. Chung, Recent membrane development for pervaporation processes, *Prog. Polym. Sci.*, 57 (2016) 1–31.
- [8] X. Zhan, J.D. Li, J.Q. Huang, C.X. Chen, Enhanced pervaporation performance of multi-layer PDMS/PVDF composite membrane for ethanol recovery from aqueous solution, *Appl. Biochem. Biotechnol.*, 160 (2010) 632–642.
- [9] J.A. León, J. Fontalvo, PDMS modified membranes by 1-dodecanol and its effect on ethanol removal by pervaporation, *Sep. Sci. Technol.*, 210 (2019) 364–370.
- [10] X. Han, L. Wang, J.D. Li, X. Zhan, J. Chen, J.C. Yang, Separation of ethanol from ethanol/water mixtures by pervaporation with silicone rubber membranes: effect of silicone rubbers, *J. Appl. Polym. Sci.*, 119 (2011) 3413–3421.
- [11] H.B. Park, J. Kamcev, L.M. Robeson, M. Elimelech, B.D. Freeman, Maximizing the right stuff: the trade-off between membrane permeability and selectivity, *Science*, 356 (2017) eaab0530.
- [12] H. Te Henneppe, D. Bargeman, M. Mulder, C. Smolders, Zeolite-filled silicone rubber membranes: part 1. Membrane preparation and pervaporation results, *J. Membr. Sci.*, 35 (1987) 39–55.
- [13] H.L. Zhou, J.Q. Zhang, Y.H. Wan, W.Q. Jin, Fabrication of high silicalite-1 content filled PDMS thin composite pervaporation membrane for the separation of ethanol from aqueous solutions, *J. Membr. Sci.*, 524 (2017) 1–11.
- [14] M.D. Jia, K.V. Peinemann, R.D. Behling, Preparation and characterization of thin-film zeolite PDMS composite membranes, *J. Membr. Sci.*, 73 (1992) 119–128.
- [15] X. Zhan, J.D. Li, J.Q. Huang, X.L. Han, Pervaporation separation of ethanol/water mixtures with chlorosilane modified silicalite-1/PDMS hybrid membranes, *Chin. J. Polym. Sci.*, 28 (2010) 625–635.
- [16] X.J. Zhuang, X.R. Chen, Y. Su, J.Q. Luo, Sh.Ch. Feng, H. Zhou, Y.H. Wan, Surface modification of silicalite-1 with alkoxysilanes to improve the performance of PDMS/silicalite-1 pervaporation membranes: preparation, characterization and modeling, *J. Membr. Sci.*, 499 (2016) 386–395.
- [17] Sh.L. Yi, Y.H. Wan, Separation performance of novel vinyltriethoxysilane (VTES)-g-silicalite-1/PDMS/PAN thin-film composite membrane in the recovery of bioethanol from fermentation broths by pervaporation, *J. Membr. Sci.*, 524 (2017) 132–140.
- [18] S. Hu, W.Q. Ren, D. Cai, T.C. Hughes, P.Y. Qin, T.W. Tan, A mixed matrix membrane for butanol pervaporation based on micron-sized silicalite-1 as macro-crosslinkers, *J. Membr. Sci.*, 533 (2017) 270–278.
- [19] L.M. Vane, V.V. Namboodiri, T.C. Bowen, Hydrophobic zeolite-silicone rubber mixed matrix membranes for ethanol-water separation: effect of zeolite and silicone component selection on pervaporation performance, *J. Membr. Sci.*, 308 (2008) 230–241.
- [20] X. Zhan, J. Lu, T.T. Tan, J.D. Li, Mixed matrix membranes with HF acid etched ZSM-5 for ethanol/water separation: preparation and pervaporation performance, *Appl. Surf. Sci.*, 259 (2012) 547–556.
- [21] Q.Q. Li, L. Cheng, J. Shen, J.Y. Shi, G.N. Chen, J. Zhao, J.G. Duan, G.P. Liu, W.Q. Jin, Improved ethanol recovery through mixed-matrix membrane with hydrophobic MAF-6 as filler, *Sep. Sci. Technol.*, 178 (2017) 105–112.
- [22] A. Khan, M. Ali, A. Ilyas, P. Naik, I.F.J. Vankelecom, M.A. Gilani, M.R. Bilad, Z. Sajjad, A.L. Khan, ZIF-67 filled PDMS mixed matrix membranes for recovery of ethanol via pervaporation, *Sep. Sci. Technol.*, 206 (2018) 50–58.
- [23] S. Xu, H. Zhang, F. Yu, X. Zhao, Y. Wang, Enhanced ethanol recovery of PDMS mixed matrix membranes with hydrophobically modified ZIF-90, *Sep. Sci. Technol.*, 206 (2018) 80–89.
- [24] H. Mao, H.G. Zhen, A. Ahmad, A.S. Zhang, Z.P. Zhi, In situ fabrication of MOF nanoparticles in PDMS membrane via interfacial synthesis for enhanced ethanol permselective pervaporation, *J. Membr. Sci.*, 573 (2019) 344–358.
- [25] N.X. Wang, G.X. Shi, J. Gao, J. Li, L. Wang, H.X. Guo, G.J. Zhang, S.L. Ji, MCM-41@ZIF-8/PDMS hybrid membranes with micro- and nanoscaled hierarchical structure for alcohol permselective pervaporation, *Sep. Sci. Technol.*, 153 (2015) 146–155.
- [26] Y.B. Li, L.H. Wee, J.A. Martens, I.F.J. Vankelecom, ZIF-71 as a potential filler to prepare pervaporation membranes for bio-alcohol recovery, *J. Mater. Chem. A*, 2 (2014) 10034–10040.
- [27] P.V. Naik, L.H. Wee, M. Meledina, S. Turner, Y.B. Li, G.V. Tendeloo, J.A. Martens, I.F.J. Vankelecom, PDMS membranes containing ZIF-coated mesoporous silica spheres for efficient ethanol recovery via pervaporation, *J. Mater. Chem. A*, 4 (2016) 12790–12798.
- [28] D. Sun, B.B. Li, Zh.L. Xu, Pervaporation of ethanol/water mixture by organophilic nano-silica filled PDMS composite membranes, *Desalination*, 322 (2013) 159–166.
- [29] H. Yan, J. Li, H. Fan, S. Ji, G. Zhang, Z. Zhang, Sonication-enhanced in situ assembly of organic/inorganic hybrid membranes: evolution of nanoparticle distribution and pervaporation performance, *J. Membr. Sci.*, 481 (2015) 94–105.
- [30] S.W. Kuo, F.C. Chang, POSS related polymer nanocomposites, *Prog. Polym. Sci.*, 36 (2011) 1649–1696.
- [31] D.Zh. Chen, Sh.P. Yi, P.F. Fang, Y.L. Zhong, Ch. Huang, X.J. Wu, Synthesis and characterization of novel room temperature vulcanized (RTV) silicone rubbers using octa[(trimethoxysilyl) ethyl]-POSS as cross-linker, *React. Funct. Polym.*, 71 (2011) 502–511.
- [32] Sh. Yang, A.Zh. Pan, L. He, Organic/inorganic hybrids by linear PDMS and caged MA-POSS for coating, *Mater. Chem. Phys.*, 153 (2015) 396–404.
- [33] N.L. Le, Y. Wang, T.Sh. Chung, Pebax/POSS mixed matrix membranes for ethanol recovery from aqueous solutions via pervaporation, *J. Membr. Sci.*, 379 (2011) 174–183.
- [34] G.P. Liu, W.S. Hung, J. Shen, Q.Q. Li, Y.H. Huang, W.Q. Jin, K.R. Lee, J.Y. Lai, Mixed matrix membranes with molecular-interaction-driven tunable free volumes for efficient bio-fuel recovery, *J. Mater. Chem. A*, 3 (2015) 4510–4521.
- [35] Q.G. Zhang, B.C. Fan, Q.L. Liu, A.M. Zhu, F.F. Shi, A novel poly(dimethyl siloxane)/poly(oligosilsesquioxanes) composite membrane for pervaporation desulfurization, *J. Membr. Sci.*, 366 (2011) 335–341.
- [36] R. Konietzny, T. Koschine, K. Rätzke, C. Staudt, POSS-hybrid membranes for the removal of sulfur aromatics by pervaporation, *Sep. Sci. Technol.*, 123 (2014) 175–182.
- [37] M.R. Wang, R.S. Xing, H. Wu, F.Sh. Pan, J.J. Zhang, H. Ding, Zh.Y. Jiang, Nanocomposite membranes based on alginate hydration and high loading of pegylated POSS for pervaporation dehydration, *J. Membr. Sci.*, 538 (2017) 86–95.
- [38] F.J. Fu, S. Zhang, Sh.P. Sun, K.Y. Wang, T.S. Chung, POSS-containing delamination-free dual-layer hollow fiber membranes for forward osmosis and osmotic power generation, *J. Membr. Sci.*, 443 (2013) 144–155.
- [39] P. Iyer, G. Iyer, M. Coleman, Gas transport properties of polyimide-POSS nanocomposites, *J. Membr. Sci.*, 358 (2010) 26–32.

- [40] F. Li, Y. Li, T.S. Chung, S. Kawi, Facilitated transport by hybrid POSS®-Matrimid®-Zn<sup>2+</sup> nanocomposite membranes for the separation of natural gas, *J. Membr. Sci.*, 356 (2010) 14–21.
- [41] Y. Li, T.S. Chung, Molecular-level mixed matrix membranes comprising Pebax and POSS for hydrogen purification via preferential CO<sub>2</sub> removal, *Int. J. Hydrogen Energy*, 35 (2010) 10560–10568.
- [42] D. Xu, L.S. Loo, K. Wang, Pervaporation performance of novel chitosan-POSS hybrid membranes: effects of POSS and operating conditions, *J. Polym. Sci., Part B: Polym. Phys.*, 48 (2010) 2185–2192.
- [43] X. Zhan, J. Lu, H. Xu, J.H. Liu, X.S. Liu, X.Z. Cao, J.D. Li, Enhanced pervaporation performance of PDMS membranes based on nano-sized Octa[(trimethoxysilyl)ethyl]-POSS as macro-crosslinker, *Appl. Surf. Sci.*, 473 (2019) 785–798.
- [44] D. Murphy, M.N. de Pinho, An ATR-FTIR study of water in cellulose acetate membranes prepared by phase inversion, *J. Membr. Sci.*, 106 (1995) 245–257.
- [45] N.J. Harrick, *Internal Reflection Spectroscopy*, Wiley, NY, 1967.
- [46] R.H. Baney, M. Itoh, A. Sakakibara, T. Suzuki, Silsesquioxanes, *Chem. Rev.*, 95 (1995) 1409–1430.
- [47] M.Q. Fang, C.L. Wu, Z.J. Yang, T. Wang, Y. Xia, J.D. Li, ZIF-8/PDMS mixed matrix membranes for propane/nitrogen mixture separation: experimental result and permeation model validation, *J. Membr. Sci.*, 474 (2015) 103–113.
- [48] X.X. Cheng, F.S. Pan, M.R. Wang, W.D. Li, Y.M. Song, G.H. Liu, H. Yang, B.X. Gao, H. Wu, Z.Y. Jiang, Hybrid membranes for pervaporation separations, 2017, *J. Membr. Sci.*, 541 (2017) 329–346.